Journal of Computational Physics **179,** 180–200 (2002)
doi:10.1006/jcph.2002.7050

Vorticity-Divergence Semi-Lagrangian Shallow-Water Model of the Sphere Based on Compact Finite Differences

Mikhail A. Tolstykh[1]

Institute of Numerical Mathematics, Russian Academy of Sciences, 8 Gubkina St., 119991 Moscow, Russia
E-mail: tolstykh@inm.ras.ru

Received February 9, 2001; revised March 5, 2002

The semi-Lagrangian representation of advection allows circumventing of the CFL restriction on time steps, which is especially severe for finite-difference models on the regular latitude–longitude grid. The distinct features of the presented semi-Lagrangian model are the use of vorticity and divergence as prognostic variables in conjunction with the fourth-order compact finite differences on the unstaggered regular latitude–longitude grid. The key point of this approach is the solution of the Poisson equations on the sphere, which is necessary for reconstructing the velocity field from vorticity and divergence. The accurate and efficient direct solver for this problem is described. The results of the standard test set for shallow-water equations on the sphere demonstrate the accuracy and computational efficiency of the model with the time steps several times greater than in the Eulerian model.

Key Words: shallow-water equations; compact finite differences; solution of the Poisson equation on the sphere; semi-Lagrangian; semi-implicit; atmospheric models.

1. INTRODUCTION

The spectral method of horizontal discretization for global atmospheric models is dominant in climate modeling and, to a smaller extent, in numerical weather prediction. As the resolution of models increases, the cost and complexity of parallel implementation of the Legendre transforms associated with the spectral method grows dramatically, and there are an increasing number of articles devoted to the alternative ways of horizontal discretization of the atmospheric equations on the sphere based on spectral element methods [22], pseudospectral methods [20], double Fourier series [3], and finite-element methods on

[1] Fax: (+7 095) 938 1821.

0021-9991/02 $35.00

icosahedral grids [5]. There are also concerns about the stability of calculation of associated Legendre functions for spectral methods for very high resolution.

Besides the obvious requirements of accuracy and computational efficiency on parallel computers, the dynamical core of a modern atmospheric model should be suitable for a variety of applications, ranging from short-term weather forecasting using variable resolution over the globe to multiyear climate simulations. Thus the possibility of using the variable resolution in at least one of the horizontal coordinates and rotated poles seems to be a desirable feature. While a rotated pole does not represent a problem, the most convenient and flexible way to implement the variable resolution feature in an atmospheric model is the finite-difference, finite-element, or finite-volume approach.

Most operational models for numerical weather prediction and some climate models, both spectral and finite difference, use the semi-Lagrangian representation of advection, which allows circumventing of the CFL restriction on time steps [21, 24, 33], which is especially severe for finite-difference models on the regular latitude–longitude grid on the sphere due to convergence of the meridians toward the pole. So, for semi-Lagrangian models the difference between spectral and finite-difference models now lies in the discretization of the horizontal nonadvective derivatives and the method for solution of the elliptic problem arising in the semi-implicit scheme.

In this paper, we present the global semi-Lagrangian finite-difference shallow-water model. The distinct features of this model are the use of vorticity and divergence as prognostic variables in conjunction with the fourth-order compact finite differences on the unstaggered regular latitude–longitude grid. These features are interrelated.

It was shown in [15, 17] for finite-difference models that the geostrophic adjustment and Rossby wave propagation are better reproduced by the unstagered grid combined with the vorticity-divergence formulation than by the standard u–v formulation on the staggered C grid. The unstaggered grid applied to the semi-Lagrangian model also allows use of a single set of trajectories for all variables (while for a staggered grid it is necessary either to use the multiple set of trajectories or to make additional interpolations).

On the other hand, the unstaggered grid makes it possible to apply easily compact high-order finite differences. Otherwise, one would need to apply high-order interpolation between half- and integer nodes of the grid (for example, to calculate the Coriolis term on the C grid).

If one uses the vorticity-divergence formulation, the wind field is obtained from the horizontal stream function and velocity potential, which are in turn obtained from the vorticity and divergence solving the Poisson equations. While this problem is trivial for spectral models, the success of a finite-difference vorticity-divergence model strongly depends on the accuracy and efficiency of this part of the model.

The results for the first version of the presented shallow-water model based on the potential vorticity equation were published in 1996 [26]. This model achieved an accuracy of the spectral model of comparable resolution with the time step four times greater than with the reference spectral Eulerian model.

However, at that time it was not clear to what extent this approach could be generalized to the 3D case. Now the SL-AV (semi-Lagrangian, absolute vorticity) 3D global atmospheric model for numerical weather prediction and potentially for climate modeling has been created and successfully validated [28, 29]. It also demonstrates good efficiency on parallel computers [28]. The SL-AV model uses absolute vorticity as one of the prognostic variables and compact finite differences on the unstaggered grid. The early versions

of the shallow-water model and SL-AV model also used fourth-order compact schemes, but the elliptic solvers for the reconstruction of the velocity field and the semi-implicit time stepping, though more accurate than standard second-order solvers, were in fact only second-order accurate. While giving good forecast scores, the SL-AV model showed some deficiencies in the surface pressure field after a six-month integration in the framework of the Held–Suarez test [7]. The problem was fixed with the implementation of a more complex algorithm yielding $O(h^3)$ global accuracy for the reconstruction of the velocity field and the semi-implicit scheme. The following 3-year integration of the dynamical core of the SL-AV model showed that the problem with the surface pressure field had disappeared. It was decided to implement all the changes in the horizontal discretization of the SL-AV model back to the shallow-water model [26], and to carry out the standard tests for shallow-water models on the sphere described in [32].

In Section 2, the basic numerical approaches are presented which are used for horizontal discretization of nonadvective terms in our global semi-Lagrangian model. In particular, we investigate the compact high-order finite-difference solver on a sphere for the problem of obtaining the wind velocities from vorticity and divergence and compare it with the conventional second-order approach. The fast Fourier transforms in the longitudinal direction are used in this part.

Section 3 describes the model, and the results of the standard test set for shallow-water models on the sphere [32] are given in Section 4.

2. RECONSTRUCTION OF THE VELOCITY FIELD FROM VORTICITY AND DIVERGENCE ON THE SPHERE

We start with the discretization of basic differential operators in the spherical coordinate system. These operators are the gradient operator,

$$\nabla f = \frac{\mathbf{i}}{a\cos\varphi}\frac{\partial f}{\partial\lambda} + \frac{\mathbf{j}}{a}\frac{\partial f}{\partial\varphi},$$

and the Laplacian operator,

$$\nabla^2 f = \frac{1}{a^2\cos^2\varphi}\frac{\partial^2 f}{\partial\lambda^2} + \frac{1}{a^2\cos\varphi}\left(\frac{\partial}{\partial\varphi}\cos\varphi\frac{\partial f}{\partial\varphi}\right)$$

where a is the Earth radius, λ the longitude, and φ the latitude.

There is also need to calculate the divergence and the vertical component of the relative vorticity from the horizontal velocity field $\mathbf{V} = (u, v)$,

$$D = \nabla\cdot\mathbf{V} = \frac{1}{a\cos\varphi}\left(\frac{\partial u}{\partial\lambda} + \frac{\partial v\cos\varphi}{\partial\varphi}\right),$$
$$\zeta = \mathbf{k}\cdot(\nabla\times\mathbf{V}) = \frac{1}{a\cos\varphi}\left(\frac{\partial v}{\partial\lambda} - \frac{\partial u\cos\varphi}{\partial\varphi}\right)$$

where $\mathbf{i}$, $\mathbf{j}$, and $\mathbf{k}$ are the unit vectors in the longitudinal, latitudinal, and vertical directions, respectively.

We use the following Padé compact scheme to discretize these operators.

$$\frac{1}{6}\left(\frac{\partial f}{\partial x}\right)_{i-1} + \frac{2}{3}\left(\frac{\partial f}{\partial x}\right)_{i} + \frac{1}{6}\left(\frac{\partial f}{\partial x}\right)_{i+1} = \frac{f_{i+1} - f_{i-1}}{2\Delta x} + O(\Delta x^4). \tag{1}$$

This scheme is also known as the Numerov scheme [16]. It can be also obtained from finite-element considerations on a uniform mesh. In atmospheric modeling, it was recently used in [20]. This formula is used to calculate the gradient and the longitudinal part of the divergence.

The grid which is used in the proposed model includes the points at the poles. Special care is taken while calculating the latitudinal component of the gradient operator near the pole singularity. In terms of Fourier expansion coefficients in longitudinal (west–east) direction, a vector field (i.e., the gradient) can have only a first coefficient not equal to zero at the poles, while a scalar field under differentiation has only a zeroth Fourier component there. The calculation of the latitudinal component of the gradient operator is carried out in Fourier space (at least near the poles). The polar value of the gradient field is defined from smoothness conditions on the latitudinal component using the interpolation of the first Fourier coefficient to the pole point.

The fourth-order formula for the longitudinal derivative in the Laplacian operator is

$$\frac{1}{12}\left(\frac{\partial^2 f}{\partial x^2}\right)_{i-1} + \frac{10}{12}\left(\frac{\partial^2 f}{\partial x^2}\right)_{i} + \frac{1}{12}\left(\frac{\partial^2 f}{\partial x^2}\right)_{i+1} = \frac{f_{i+1} - 2f_i + f_{i-1}}{\Delta x^2} + O(\Delta x^4). \tag{2}$$

To discretize the latitudinal component of the Laplacian and divergence operators, the following approximation to the first derivative is used (e.g., [9]):

$$\frac{1}{24}\left(\frac{\partial f}{\partial x}\right)_{i-1} + \frac{11}{12}\left(\frac{\partial f}{\partial x}\right)_{i} + \frac{1}{24}\left(\frac{\partial f}{\partial x}\right)_{i+1} = \frac{f_{i+1/2} - f_{i-1/2}}{\Delta x} + O(\Delta x^4). \tag{3}$$

This formula can be rewritten in symbolic form as

$$\frac{\partial f}{\partial x} = M^{-1}\delta f,$$

where M is the symmetric tridiagonal operator with diagonals $(1/24, 11/12, 1/24)$ and $\delta f = \frac{f_{i+1/2} - f_{i-1/2}}{\Delta x}$.

One can see that Eq. (3) involves half-nodes of the grid. One can show that successive application of (3) to the discretization of the first derivatives in the latitudinal component of the Laplacian results in the fourth-order-accurate conservative scheme.

Consider now the application of the fourth-order compact finite differences to the solution of the Poisson equation on the sphere:

$$\frac{1}{a^2\cos^2\varphi}\frac{\partial^2 g}{\partial \lambda^2} + \frac{1}{a^2\cos\varphi}\left(\frac{\partial}{\partial \varphi}\cos\varphi\frac{\partial g}{\partial \varphi}\right) = F. \tag{4}$$

Of course, it is expensive to implement this approach in a straightforward way in the multidimensional problem. We use the Fourier representation in the longitudinal direction in the solver, replacing compact finite differences in this direction by their Fourier images (see the second-order solver in [14] and references herein). For example, to differentiate

some function f in longitude equivalently to (1), we have to multiply each complex Fourier coefficient $\hat{f}_k$ by $i\langle k\rangle$, where

$$\langle k\rangle = \frac{\sin(k\Delta\lambda)}{\Delta\lambda(1 - 2/3\sin^2(k\Delta\lambda/2))}$$

and $i = \sqrt{-1}$, $\Delta\lambda$ is the mesh size in longitude.

Similarly, to calculate the second derivative, each Fourier coefficient is multiplied by $-\langle k^2\rangle$ with

$$\langle k^2\rangle = \frac{4\sin^2\left(\frac{k\Delta\lambda}{2}\right)}{\Delta\lambda^2(1 - 1/3\sin^2(k\Delta\lambda/2))}.$$

The longitudinal derivatives are evaluated with the above formulas instead of exact differentiation in Fourier space to be consistent with the rest of the model, where these derivatives are calculated using compact finite differences. In doing so, we also preserve the invariance of the discretized Laplacian operator near the equator with respect to pole rotation of the spherical coordinate system (up to fourth-order terms).

We write the discretization of the Poisson equation (4) for a nonzero longitudinal wavenumber k apart from the poles and near pole rows as

$$-\frac{\langle k^2\rangle}{\cos\varphi_j}\hat{g}^k_j + M^{-1}\delta\left(\cos\varphi_j M^{-1}\delta\hat{g}^k_j\right) = a^2\cos\varphi_j\hat{F}^k_j,$$

where j is the latitudinal index and $\hat{g}^k$ and $\hat{F}^k$ are the kth Fourier components of g and F, respectively. The grid in latitude includes the points at the poles, which have the indices 0 and N.

Introducing an auxiliary variable $\hat{z} = M^{-1}\delta\hat{g}$, this equation can be cast into the system of two equations,

$$\begin{cases} -M\left(\frac{\langle k^2\rangle}{\cos\varphi_j}\right)\hat{g}^k_j + \delta\left(\hat{z}^k_j\cos\varphi_j\right) = a^2 M\left(\hat{F}^k_j\cos\varphi_j\right) \\ -\delta\hat{g}^k_j + M\hat{z}^k_j = 0 \end{cases} \tag{5}$$

or

$$A_j\begin{pmatrix}\hat{g}^k\\ \hat{z}^k\end{pmatrix}_{j-1} + B_j\begin{pmatrix}\hat{g}^k\\ \hat{z}^k\end{pmatrix}_{j} + C_j\begin{pmatrix}\hat{g}^k\\ \hat{z}^k\end{pmatrix}_{j+1} = \begin{pmatrix}\hat{G}^k_j\\ 0\end{pmatrix},$$

where

$$A_j = \begin{pmatrix} \frac{-\langle k^2\rangle\Delta\varphi}{24\cos\varphi_{j-1}} & -\cos\varphi_{j-1/2} \\ 0 & \frac{1}{24}\end{pmatrix}, \quad B_j = \begin{pmatrix} \frac{-11\langle k^2\rangle\Delta\varphi}{12\cos\varphi_j} & \cos\varphi_{j+1/2} \\ \frac{1}{\Delta\varphi} & \frac{11}{12}\end{pmatrix},$$

$$C_j = \begin{pmatrix} \frac{-\langle k^2\rangle\Delta\varphi}{24\cos\varphi_{j+1}} & 0 \\ \frac{-1}{\Delta\varphi} & \frac{1}{24}\end{pmatrix},$$

$$\hat{G}^k_j = a^2\Delta\varphi\left(\frac{1}{24}\hat{F}^k_{j-1}\cos\varphi_{j-1} + \frac{11}{12}\hat{F}^k_j\cos\varphi_j + \frac{1}{24}\hat{F}^k_{j+1}\cos\varphi_{j+1}\right),$$

$$j = 2, 3, \ldots, N-2.$$

Note that actually $\hat{z}_j^k$ is defined at half-nodes of the grid, but for convenience we assign an integer index to it, so that the index j for $\hat{z}_j^k$ runs from 0 to $N-1$, while it changes from 0 to N for $\hat{g}_j^k$.

Near the poles, Eq. (5) is modified to avoid division by a zero value of $\cos\varphi$ at the poles. The resulting order of accuracy is thus reduced to third. At the poles, a scalar function can have only a zeroth Fourier coefficient not equal to zero; so the boundary conditions for $\hat{g}^k$ are simply $\hat{g}_0^k = 0$. For $\hat{z}_0^k$ (defined as half a grid step away from the pole), we use the condition of symmetry. This results in the following matrices (example for the southern pole):

$$A_1 = \begin{pmatrix} 0 & -\cos\varphi_{1/2} \\ 0 & \frac{1}{24} \end{pmatrix}, \quad B_1 = \begin{pmatrix} \frac{-11\langle k^2\rangle\Delta\varphi}{12\cos\varphi_1} & \cos\varphi_{3/2} \\ \frac{1}{\Delta\varphi} & \frac{11}{12} \end{pmatrix}, \quad C_1 = \begin{pmatrix} \frac{-\langle k^2\rangle\Delta\varphi}{24\cos\varphi_2} & 0 \\ \frac{-1}{\Delta\varphi} & \frac{1}{24} \end{pmatrix}.$$

$$B_0 = \begin{pmatrix} 1 & 0 \\ \frac{1}{\Delta\varphi} & \frac{23}{24} \end{pmatrix}, \quad C_0 = \begin{pmatrix} 0 & 0 \\ \frac{-1}{\Delta\varphi} & \frac{1}{24} \end{pmatrix}, \quad \hat{G}_0^k = 0.$$

This system is solved with a 2×2 block-tridiagonal version of Gaussian elimination. We precompute and store the coefficients necessary for matrix inversion that do not change in time.

The case of longitudinal wavenumber $k = 0$ is considered separately, depending on the equation to be solved, and is described further.

Consider now the problem of reconstruction of the wind velocity field from the vorticity and divergence on the sphere. First, the pair of Poisson equations on the sphere is solved to find the streamfunction ψ and velocity potential χ from known vorticity ζ and divergence D:

$$\nabla^2\psi = \zeta, \tag{6}$$

$$\nabla^2\chi = D. \tag{7}$$

Then the horizontal velocity components u and v are restored using the Helmholtz theorem:

$$u = -\frac{1}{a}\frac{\partial\psi}{\partial\varphi} + \frac{1}{a\cos\varphi}\frac{\partial\chi}{\partial\lambda}, \tag{8}$$

$$v = \frac{1}{a\cos\varphi}\frac{\partial\psi}{\partial\lambda} + \frac{1}{a}\frac{\partial\chi}{\partial\varphi}. \tag{9}$$

The solution of the Poisson equations and the differentiation of the streamfunction and velocity potential is carried out in Fourier space. The result is then transformed back to the grid-point space.

Consider now the solution of Eqs. (6)–(9) for the 0th Fourier component. All longitudinal derivatives vanish. We do not need $\hat{\psi}^0$ and $\hat{\chi}^0$ but we need their latitudinal derivatives at integer nodes of the grid. Hence each pair of Eqs. (6), (8) and (7), (9) can be reduced to a single equation for

$$\hat{u}^0 = -\frac{1}{a}\frac{\partial\hat{\psi}^0}{\partial\varphi}, \quad \hat{v}^0 = \frac{1}{a}\frac{\partial\hat{\chi}^0}{\partial\varphi}.$$

They read

$$\frac{1}{a\cos\varphi}\frac{\partial}{\partial\varphi}(\hat{u}^0\cos\varphi) = -\hat{\zeta}^0, \tag{10}$$

$$\frac{1}{a\cos\varphi}\frac{\partial}{\partial\varphi}(\hat{v}^0\cos\varphi) = \hat{D}^0. \tag{11}$$

Their discretization with the operator $M^{-1}\delta$ can be written as

$$\delta(\hat{u}^0\cos\varphi) = -aM(\hat{\zeta}^0\cos\varphi),$$
$$\delta(\hat{v}^0\cos\varphi) = aM(\hat{D}^0\cos\varphi).$$

Here $\hat{\zeta}^0$ and $\hat{D}^0$ are defined at the integer nodes of the grid, while $\hat{u}^0$, $\hat{v}^0$ are defined at half-nodes. Third-order boundary conditions for these equations are derived using the third-order formula

$$\left(\frac{\partial f}{\partial x}\right)_{i+1} - \left(\frac{\partial f}{\partial x}\right)_{i} = \frac{4}{\Delta x}\left(f_i - 2f_{i+1/2} + f_{i+1}\right) + O(\Delta x^3),$$

taking into account the fact that $\hat{u}^0$, $\hat{v}^0$ are equal to zero at the poles. Having obtained $\hat{u}^0$ and $\hat{v}^0$ at half-nodes of the grid, we interpolate them with the sixth-order compact interpolation [9] to the integer nodes. The reason the sixth-order interpolation is used here is the very high sensitivity of errors to the choice of interpolation. The fourth-order compact interpolation was found to be insufficient to provide good error measures.

To solve Eqs. (8) and (9) for nonzero Fourier coefficients, both functions $\hat{g}$ and $\hat{z}$ from Eq. (5) are needed. The latter is interpolated from half-nodes to integer nodes using again the sixth-order compact interpolation.

We first use the known analytic solution to compare our approach with the standard second-order finite differences. The second-order solver for the elliptic-type equations on the sphere based on Fourier expansion in longitude is described in [14]. It is supplemented by the second-order central differences for differentiation of the streamfunction and velocity potential. Further, this solver is referred to as the standard solver.

In the analytic case, the vorticity and divergence are known in advance. The velocity field to be restored is the initial velocity of the Rossby–Haurwitz wave number 4 [32].

$$\begin{aligned} u &= a\omega\cos\varphi(1 + \cos^2\varphi(4\sin^2\varphi - \cos^2\varphi)\cos 4\lambda), \\ v &= -4a\omega\cos^3\varphi\sin\varphi\sin 4\lambda, \end{aligned} \tag{12}$$

and the associated vorticity and divergence are

$$\zeta = \omega\sin\varphi(2 - 30\cos^4\varphi\cos 4\lambda), \quad D = 0, \tag{13}$$

where $\omega = 7.848 \times 10^{-6}$.

The calculations were carried out with the horizontal resolution in longitude and latitude of 0.75, 1, 1.5, 2, and 2.5 degrees (241, 181, 121, 91, and 73 points along latitude, respectively). The obtained velocity field was compared with the known analytical field; namely, the normalized l_2 errors (defined in [32]) for u and v components were calculated.

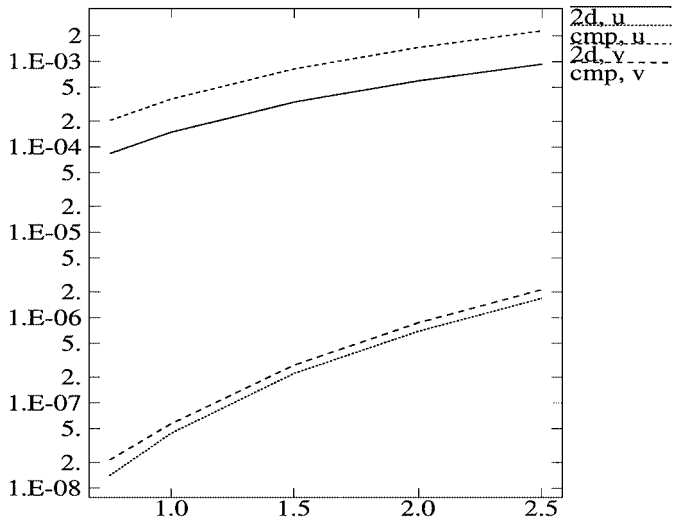

FIG. 1. Normalized l_2 errors of u and v fields as functions of resolution (in degrees) for Rossby–Haurwitz test solutions (2D, solver based on second-order central differences; cmp, solver based on compact schemes).

The results given in Fig. 1 confirm the advantages of the proposed algorithm over the standard second-order solver. They also show that the proposed algorithm demonstrates the third-order convergence.

Another test was carried out using the artificial distribution with the strong cross-polar flow [1]. In this case,

$$u = U_0(\sin\varphi(\sin^2\varphi - 3\cos^2\varphi)\sin\lambda - 0.5\cos\varphi),$$
$$v = U_0 \sin^2\varphi\cos\lambda,$$

and the associated vorticity and divergence are

$$\zeta = \frac{U_0}{a}(\cos\varphi(16\cos^2\varphi - 13)\sin\lambda - \sin\varphi),$$
$$D = -\frac{U_0}{a}\cos\lambda\sin\varphi\cos\varphi,$$

where $U_0 = 30$ m/s.

The same error measures for this test are given in Fig. 2. One can see again that the proposed solver demonstrates significantly better accuracy than the standard second-order scheme.

This test was repeated with the real data winds for 500 hPa on the 15th of January, 1996, extracted from the archives of the European Center for Medium Range Weather Forecasts (ECMWF). The resolution was fixed at 1.5 degrees. In this case, the vorticity and divergence were calculated numerically using sixth-order compact differencing. The results, including the normalized mean error for the u component of the wind (which gives rise to the change in angular momentum of the atmosphere) are given in Table I. Again we observe the advantage of the proposed solver over the second-order scheme. In this case, the difference between two methods is smaller, since the numerical differentiation of velocity field introduces some error, equal for both solvers.

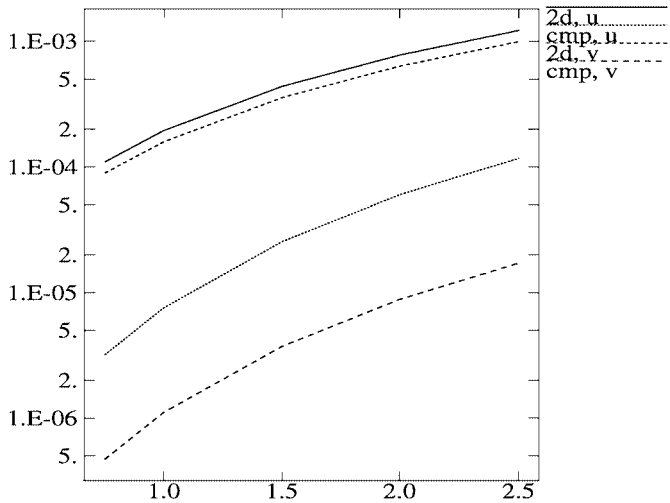

FIG. 2. Normalized l_2 errors of u and v fields as functions of resolution (in degrees) for cross-polar flow test solutions (2D, solver based on second-order central differences; cmp, solver based on compact schemes).

Considering geographical distribution of errors in all considered cases, one can note that maximums of errors are localized at near-pole rows (not shown). The magnitude of error in all areas except two to three near-pole rows of the grid is 3–10 times less (depending on the test case) than the maximum value.

Now we compare the cost of the proposed and standard solvers for the reconstruction of velocity. If all coefficients that do not depend on the right-hand side are precomputed and stored, the solution of the Poisson equation for a given Fourier component requires 21 floating-point operations per latitudinal grid point, while the standard solver requires only five operations. The differentiation of the streamfunction and velocity potential in Fourier space adds 11 operations for the proposed scheme and four operations for the standard solver (per equation). Both solvers need direct and inverse fast Fourier transforms (FFT). The cost of a single FFT can be approximately estimated as $4N(\log_2 N)$ operations (depending on factors which compose N; see [30]), which gives 29 operations per grid point for 2 degrees of resolution. So the cost of the compact scheme in the considered problem is partially masked by the cost of the FFTs. For the resolutions considered, the solver based on compact schemes is less than 1.5 times more expensive than the second-order one. This price seems to be affordable, given the accuracy of the suggested scheme, which is at least four times higher for real fields (three to four orders of magnitude for smooth fields). Thus, at worst, the proposed solver is 2.6 times more efficient than the standard one. The efficiency increases with the increase in the resolution due to the higher convergence rate of the proposed scheme and the relative increase in the FFT cost.

TABLE I

Normalized l_2, Maximum, and Mean Errors for Real-Data Winds

Solver	$ERR_2(u)$	$ERR_\infty(u)$	$ERR_2(v)$	$ERR_\infty(v)$	$ERR_M(u)$
Second order	0.0109	0.0251	0.0126	0.0223	3.49×10^{-4}
Compact	0.00103	0.00916	0.00143	0.00627	6.43×10^{-5}

3. FORMULATION OF THE SHALLOW-WATER MODEL AND ITS DISCRETIZATION

The first semi-Lagrangian shallow-water model that used potential vorticity as one of prognostic variables was [23]. Bates *et al*. [2] created the global shallow-water potential-vorticity-based model using the nonlinear discrete formulation. The idea was that the use of the potential vorticity combined with the nonlinear continuity equation could give a better representation of nonlinear atmospheric dynamics. They used the multigrid technique to solve a coupled system of nonlinear equations. The results of the 1-month integration of the Rossby–Haurwitz wave number 4 were promising. However, it is difficult to generalize this approach to the 3D case. In our global shallow-water model, the absolute vorticity is used as one of the prognostic variables. Momentum equations written in the vector form are used to obtain the RHS of the divergence equation, as we want to avoid the appearance of the metric terms. Using the momentum equations, the metric terms are absorbed in the rotation operators, as described in [1]. Explicit integration of these terms would lead to instability. The so-called "advected" Coriolis term suggested in 1990 by Rochas [18] is used in the momentum equations, which allows use of the coordinate system with the rotated pole in the two-time-level semi-Lagrangian semi-implicit discretization without loss of stability.

We start with the shallow-water equations on the sphere written with the modification proposed in [19] aimed to suppress the spurious orographic resonance in the discretized semi-Lagrangian equations. They are the absolute vorticity equation

$$\frac{d(\zeta + f)}{dt} = -(\zeta + f)D.$$

Momentum equations written in the vector form on the sphere are used only to obtain the right-hand side for the discrete divergence equation,

$$\left(\frac{d(\mathbf{V} + 2\Omega \times \mathbf{r})}{dt}\right)_H = -\nabla\Phi - \nabla\Phi_s. \tag{14}$$

The continuity equation is written as

$$\frac{d(\Phi + \Phi_s)}{dt} = -\Phi D + \mathbf{V} \cdot \nabla\Phi_s.$$

Here $\mathbf{r}$ is the radius vector of the current point ($\Omega \times \mathbf{r} = (|\Omega| a \cos\varphi, 0)$ if the poles of geographical and computational grids coincide), Φ is the depth of the fluid multiplied by g, Φ_s is the surface geopotential (height of the mountains multiplied by g), Ω is the vector of angular velocity of Earth's rotation directed through the Northern pole, $f = 2|\Omega| \sin\varphi$ is the the Coriolis parameter, $\mathbf{V}$ is the horizontal velocity vector, D is the divergence, d/dt is the three-dimensional Lagrangian derivative, and

$$\left(\frac{d\mathbf{V}}{dt}\right)_H = \text{ horizontal projection of } \left(\frac{d\mathbf{V}}{dt}\right).$$

The temporal discretization is based on the two-time-level scheme, with the extrapolation of nonlinear terms in the continuity, the vorticity equations to the intermediate time level $n + 1/2$, and the linearized treatment of fast gravity waves (semi-implicit scheme) leading to Helmholtz-type equations to be solved at each time step. Such discretization is described in detail in [1]. We use the temporal decentering in the divergence and continuity equations

while using a centered-in-time scheme for the voriticity equation, as in [11], to suppress the spurious orographic resonance intrinsic to the semi-Lagrangian models [19].

The temporal discretization of the governing equations is as follows (the asterisk denotes the values at the departure points of trajectories).
The absolute vorticity equation is

$$\zeta^{n+1} + f\left(1 + \frac{\Delta t}{2} D\right)^{n+1} = \zeta_*^n + f_*\left(1 - \frac{\Delta t}{2} D\right)_*^n - \frac{\Delta t}{2}(\zeta D)_*^{n+1/2} - \frac{\Delta t}{2}(\zeta D)^{n+1/2}. \tag{15}$$

The discrete divergence equation is written as

$$D^{n+1} = -\frac{1+\epsilon}{2}\Delta t \nabla^2(\Phi'^{n+1} + \Phi_s) + \tilde{A}, \tag{16}$$

where ϵ is a small first-order decentering parameter, Δt is the time step, and

$$\tilde{A} = \frac{1}{a\cos\varphi}\left(\frac{\partial A_\lambda}{\partial \lambda} + \frac{\partial A_\varphi \cos\varphi}{\partial \varphi}\right),$$
$$A_\lambda = \alpha_1 R_{u*}^n + \alpha_2 R_{v*}^n - 2|\Omega| a \cos\varphi^{n+1}, \quad A_\varphi = -\alpha_2 R_{u*}^n + \alpha_1 R_{v*}^n,$$

for the case when the poles of geographical and computational grids coincide. R_{u*}^n and R_{v*}^n are known quantities of the momentum equations at the nth time step evaluated at the departure point

$$\left(R_{u*}^n, R_{v*}^n\right) = (\mathbf{V} + 2\Omega \times \mathbf{r})_*^n - \frac{1-\epsilon}{2}\Delta t(\nabla\Phi + \nabla\Phi_s)_*^n,$$

and α_1 and α_2 describe the change of orientation of a vector at the departure point as seen from the arrival point [1].

One can note that if one uses high-order finite differences on the unstaggered grid, the curl of the discretized momentum equations (14) may not be consistent with Eq. (15). Indeed, in this case it is very difficult to obtain an exact cancellation between the cross-derivatives of Φ.

Finally, the continuity equation is discretized as follows:

$$\frac{(\Phi'^{n+1} + \Phi_s) - (\Phi'^n + \Phi_s)_*}{\Delta t}$$
$$= -\frac{1+\epsilon}{2}\left(\bar{\Phi} D^{n+1} + (\Phi' D)^{n+1/2}\right) - \frac{1-\epsilon}{2}\left(\bar{\Phi} D_*^n - (\Phi' D)_*^{n+1/2}\right)$$
$$+ \frac{1+\epsilon}{2}\mathbf{V}^{n+1/2} \cdot \nabla\Phi_s + \frac{1-\epsilon}{2}\left(\mathbf{V}^{n+1/2} \cdot \nabla\Phi_s\right)_*. \tag{17}$$

Here $\Phi' = \Phi - \bar{\Phi}$, where $\bar{\Phi}$ is the reference height.

The values at the intermediate time level $n + 1/2$ for some function p are obtained from the extrapolation $p^{n+1/2} = 3/2p^n - 1/2p^{n-1}$ Such extrapolation is also used to obtain the velocity components at time $n + 1/2$ necessary to find the departure points. The linear terms are averaged along the semi-Lagrangian trajectory, while the nonlinear terms are averaged between the departure and arrival points at time level $n + 1/2$. Note that such extrapolations can be unstable [13]. Indeed, the instability was found in the high-resolution 3D models, mostly when applied to the vertical component of velocity [4].

In the global shallow-water model based on potential vorticity equation [2], it was found necessary to use the linearized treatment of the Coriolis parameter in the vorticity equation to prevent the instability (also originating from the use of a time-extrapolated wind field to determine the departure points). This problem is solved as in [26], by separating the Coriolis parameter to be estimated at the departure point from the other terms of this equation. Then, rather than interpolate it, we calculate it analytically from the known latitude of the departure point. This requires an additional interpolation for the term $(1 - \frac{\Delta t}{2} D)^n_*$ (see also [6, 13] for the analysis and development of stable two-time-level semi-Lagrangian schemes).

Using (16) to eliminate D^{n+1} from Eq. (17), we obtain the Helmholtz equation for Φ' to be solved at each time step.

$$\nabla^2 \Phi'^{n+1} - \mu^2 \Phi'^{n+1} = H,$$

where

$$\mu^2 = \left[\left(\frac{1+\epsilon}{2} \Delta t \right)^2 \bar{\Phi} \right]^{-1},$$

$$H = \mu^2 \left(\frac{1-\epsilon}{2} \bar{\Phi} \Delta t \left(\tilde{A} - \frac{1+\epsilon}{2} \Delta t \nabla^2 \Phi_s \right) + B_\Phi \right),$$

and where B_Φ represents the known terms of the continuity equation (similar to B_u, B_v). This equation is discretized in Fourier space in a way similar to the Poisson equation described in the previous section.

At the poles, we make use of the fact that the scalar field Φ' can have only a zeroth Fourier coefficient not equal to zero. The resulting tridiagonal 2×2 matrix equation with complex unknowns is solved for each Fourier harmonic using the block-tridiagonal Gauss elimination. Again, all the coefficients for matrix inversion that do not change with time are precomputed and stored.

The next step is to obtain D^{n+1} and relative vorticity ζ^{n+1} from (17) and (15), respectively. Then the horizontal velocity field is restored using the algorithm presented in the previous section.

The model includes the implicit fourth-order diffusion acting on the divergence field only, implemented in Fourier space with the finite-volume representation in latitude [27]. This algorithm, allowing variable resolution in latitude, is a generalization of the one presented in [10]. The implicit fourth-order diffusion equation is reduced to the system of two second-order equations, which is solved using 2×2 block-tridiagonal matrix inversion in latitude. As the divergence field is already in Fourier space, there is no additional Fourier transforms. This diffusion acts in a way similar to the filters described in [20]. For other fields, the intrinsic diffusion of the interpolation process was found to be sufficient.

The implementation of the model is organized as follows. Calculations in the grid-point space consist of the computations of the quantities from Eqs. (15)–(17) at time level n, the

trajectory search algorithm, and the interpolations of these quantities. Then the direct fast Fourier transforms for the interpolated quantities follow. The semi-implicit time stepping, the reconstruction of the horizontal velocity from the divergence and vorticity, and the horizontal diffusion of divergence are carried out in the space of longitudinal Fourier coefficients. Finally, the inverse fast Fourier transforms restore grid-point values of prognostic variables.

In the semi-Lagrangian advection part, the cubic spline interpolation with the approximate inversion of the tridiagonal operators is used to calculate the quantities at departure points of trajectories. The approximate inversion allows use of a limited stencil of interpolation, which facilitates the parallel implementation of the full 3D model.

The algorithm for finding the departure points of trajectories on the sphere is described in [34]. The linear interpolations are used to estimate extrapolated velocities at the midpoints of trajectories.

Let us discuss the cost of the proposed scheme with respect to the known methods. Clearly, it is more expensive than the classical u–v second-order finite-difference semi-Lagrangian model using the staggered C grid—the integration of vorticity and divergence equations requires two interpolations of quantities at the departure point per equation (while for the u–v model one interpolation per u and v equation is sufficient). One also needs to reconstruct the velocity field from divergence and vorticity. However, in the full 28-level 3D SL-AV model, including the parameterizations of the subgrid scale processes (which account for 60.5% of total CPU time of the model), the cost of the solver for the reconstruction of velocities (including the cost of additional fast Fourier transforms) was found to be 2.2%. The cost of integration of the vorticity equation (which looks more complex in the 3D case) is 5.3%. These costs seems to be affordable, given that for most complex tests from the set [32] the proposed scheme is more accurate and efficient than the classical finite-difference model (see below). On the other hand, the proposed model is clearly more efficient than the spectral semi-Lagrangian model, especially for high resolutions, where the cost of the Legendre transforms in the spectral method grows dramatically. It is also somewhat easier to implement on parallel computers with distributed memory, as the load balancing of computations in the spectral space is very complicated due to the commonly used triangular truncation.

4. RESULTS OF THE STANDARD TEST SET FOR SHALLOW-WATER MODELS

Here we describe the results for the standard test set for shallow-water equations on the sphere [32].

As was discussed in [33], for a climate model with low resolution, there is no benefit from using the semi-Lagrangian advection. So the tests were carried out using the resolutions of 2.5, 2, and 1.5 degree in longitude and latitude. We compare our results with the reference spectral Eulerian semi-implicit model [8] and explicit Eulerian models with the usual, compact finite difference and Fourier derivative calculations and twisted icosahedral grid [20, 22]. These papers contain error measures for all tests from [32].

The time step is 1 h for 2.5 and 2 degrees of resolutions; for the resolution of 1.5 degrees the time step is 45 min. The initial states were initialized using the digital filter initialization [12] with a cutoff period of 6 h. The normalized l_2 height errors at the end of all tests for different resolutions are summarized in Table II. For cases from 2 to 4, the normalized l_2 errors are given between the computed and the analytic height field. For cases 5–7, there is

TABLE II
Normalized l_2 Height Errors

Resolution	Test 2	Test 3	Test 4	Test 5	Test 6	Test 7a
2.5	4.3×10^{-4}	5.1×10^{-4}	0.014	0.0056	0.0052	0.0027
2	3.1×10^{-4}	4.1×10^{-4}	0.0096	0.0054	0.0029	0.0017
1.5	2.3×10^{-4}	3.2×10^{-4}	0.007	0.0054	0.0016	0.0013

no analytic solution and the results from the NCAR high-resolution (T213) spectral semi-implicit model are used as a reference [8]. The results of test case 1 for semi-Lagrangian advection algorithm with different interpolations at the departure point were extensively discussed in [31], so they are not presented here. Note, however, that the cubic spline interpolation used in this model gives smaller errors than conventional cubic Lagrange interpolations.

Test case 2 is a steady-state solution for global nonlinear zonal geostrophic flow. We ran it for the case $\alpha = \pi/4$ (where α is the angle between the pole of the computational grid and the axis of solid body rotation) to enable a comparison with the results described in [20, 22]. This is a trivial problem for the spectral method, since the solution is represented exactly by the basis functions. Not surprisingly, the error measures of the presented model are significantly higher for this test (see Fig. 3, left panel). The normalized l_2 height error for different resolutions demonstrates the second-order convergence, since the accuracy of our model here is limited to that of the algorithm for a trajectory search.

For a Lagrange–Galerkin scheme on the icosahedral grid, this error is somewhat larger [5], with a slower convergence rate. (Note that the angle α is not specified in [5].)

Test case 3 is similar to test case 2 except that the wind field is nonzero in a limited region. Due to the local nature of the semi-Lagrangian advection algorithm, the increase in error with respect to the previous test is significantly smaller than for any spectral or spectral-like method [20, 22] but still the error is much larger than for methods described in the mentioned papers (Fig. 3, right panel).

As was mentioned in [8], the numerical schemes alternative to the spectral method do not have to perform as well at these tests to be considered viable for practical applications.

Test case 4 is a forced nonlinear system with a translating low. The velocity parameter was $u_0 = 20$ m/s. The forcing for the vorticity equation is calculated by applying the *curl* operator to the forcing for the momentum equations. The second-order accuracy in time requires the forcing to be averaged along the semi-Lagrangian trajectory. Since the momentum equations are written in the vector form on the sphere, the metric terms are absent in the discrete equation (16). In order to avoid an inconsistency between the forcing [32], where these term are present, and Eq. (15), we replace the original forcing with its semi-Lagrangian form discretized in time. It was noted in [20] that the time truncation error is dominant in this test. Indeed, the graphs of the l_2 height error for different resolutions show little difference (Fig. 3, lower panel). As the forcing is modified, the direct comparison with the results of [20, 22] is not possible.

Test case 5 is zonal flow over an isolated mountain. Here we cannot obtain good convergence to the reference solution, for two reasons. First, the zonal flow initial condition is not in geostrophic equilibrium with the topography, resulting in gravity waves of significant amplitude. These waves are poorly resolved by the semi-implicit reference solution, and the

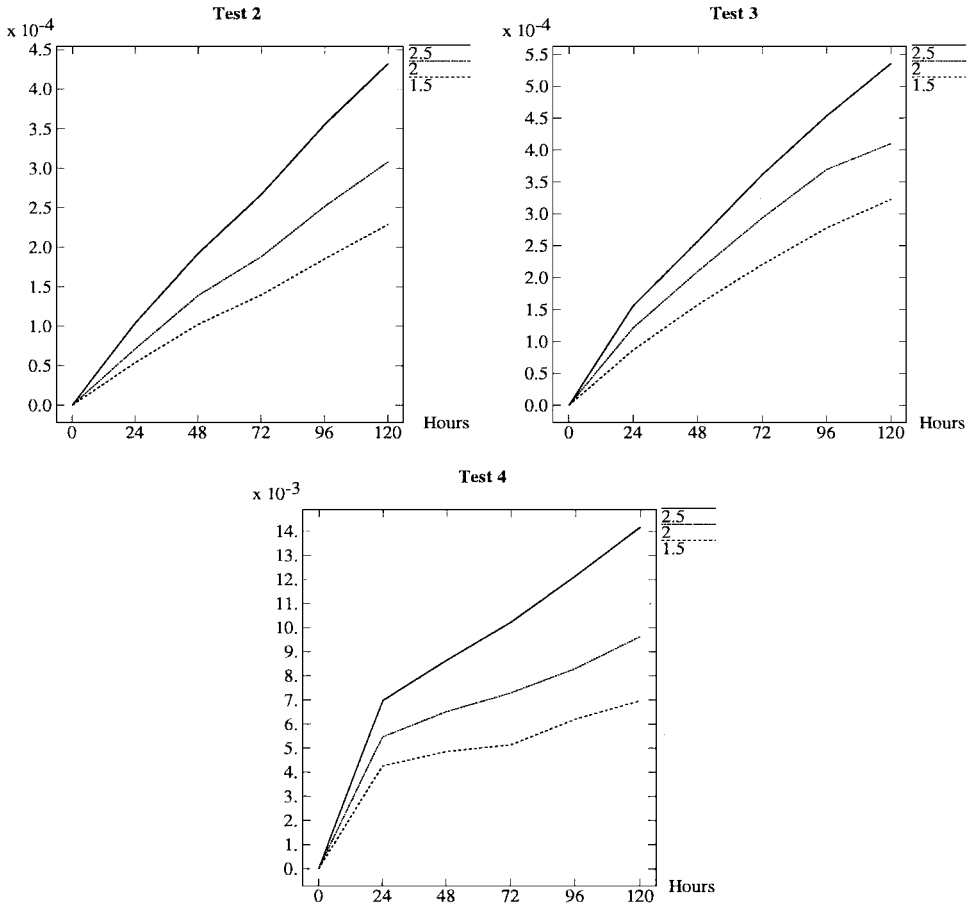

FIG. 3. Normalized l_2 height errors for tests 2–4 with different resolutions (in degrees).

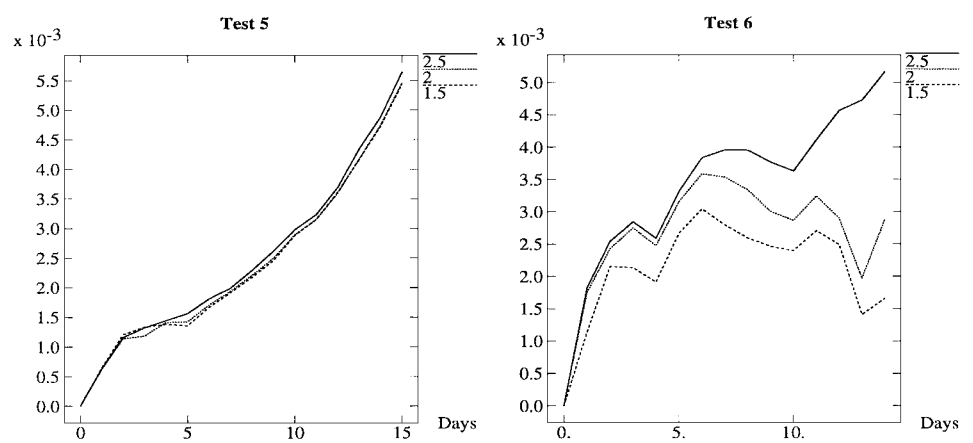

FIG. 4. Normalized l_2 height errors for tests 5 and 6 with different resolutions (in degrees).

l_2 height error for any method has an uncertainty of about 10^{-3} [22]. Second, the specified orography (which is not continuously differentiable) cannot be accurately represented by the spectral method. The normalized l_2 height error of the presented model is of the order of mentioned uncertainty (Fig. 4, left panel). In this test, the initialization was omitted.

Test case 6 is the Rossby–Haurwitz wave number 4 (Eqs. (12) and (13)). The graphs of the temporal evolution of the normalized l_2 height error are depicted in Fig. 4 (right panel). The model was found to maintain the initial shape of this wave for at least 1 month. The initial global field of geopotential height and its shape after 1, 7, and 14 days of model integration are shown in Figs. 5 and 6, respectively. (See [25] for a discussion about shape of Rossby–Haurwitz wave in different models.)

The normalized l_2 height error is 1.5 times higher for our model with 1.5 degrees of resolution (time step-45 min) than for a spectral method with a slightly higher resolution,

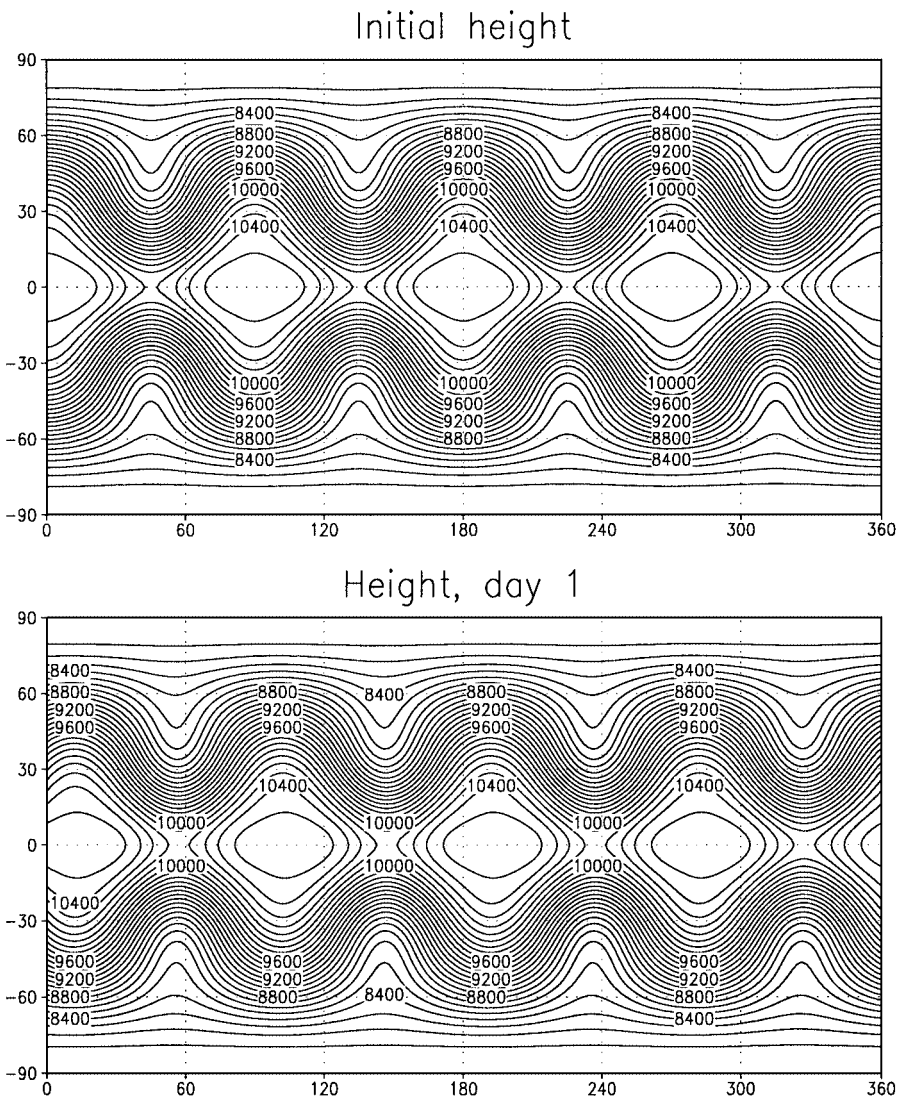

FIG. 5. Initial height field of geopotential height (m) for Rossby–Haurwitz wave (test 6) and its shape after 1 day of integration (2 degrees of resolution).

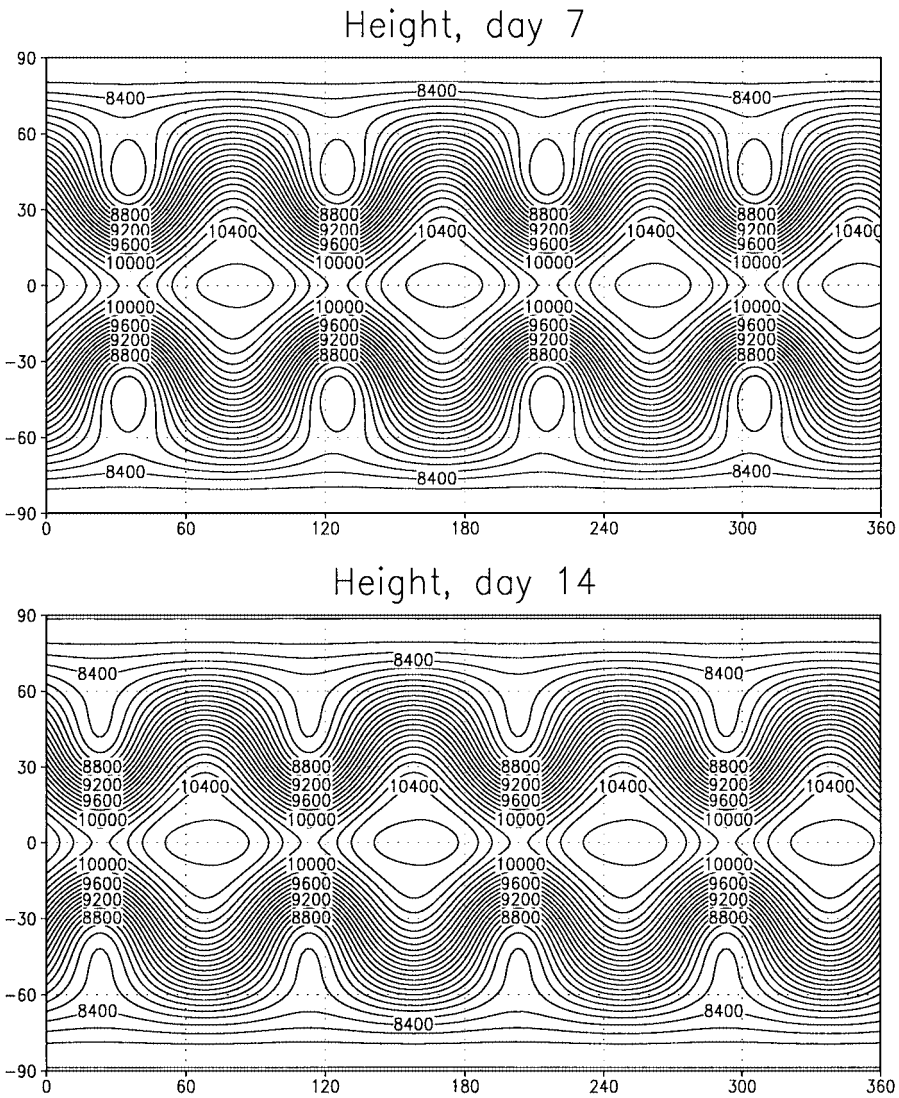

FIG. 6. Evolution of Rossby–Haurwitz wave (test 6) after 7 and 14 days of integration. (2 degrees of resolution).

T85, and explicit time stepping (time step-90 s) [20] but about two times lower than for a spectral model with a (closest lower) resolution of T63, semi-implicit time stepping, and a time step of 15 min [8]. Consider now the results of the presented model with 2.5 degrees of resolution, which is equivalent to a T42 spectral resolution. In our model with the time step of 1 h, the normalized l_2 height error after 14 days (0.0052) is slightly larger than for a spectral model with the explicit time stepping and a time step of 3 min (0.0044) but is nearly the same as for a semi-implicit spectral model with a time step of 20 min (0.0054). The uncertainty of the l_2 norm for this test is about 0.0008 [22]. Note also that for the spectral method the representation of the initial condition in this test is trivial. Comparing the result of this test with the explicit finite-difference u–v Arakawa–Lamb model, one can note that the proposed scheme is two times more accurate than the Arakawa–Lamb model with the same resolution of 2.5 degrees [22].

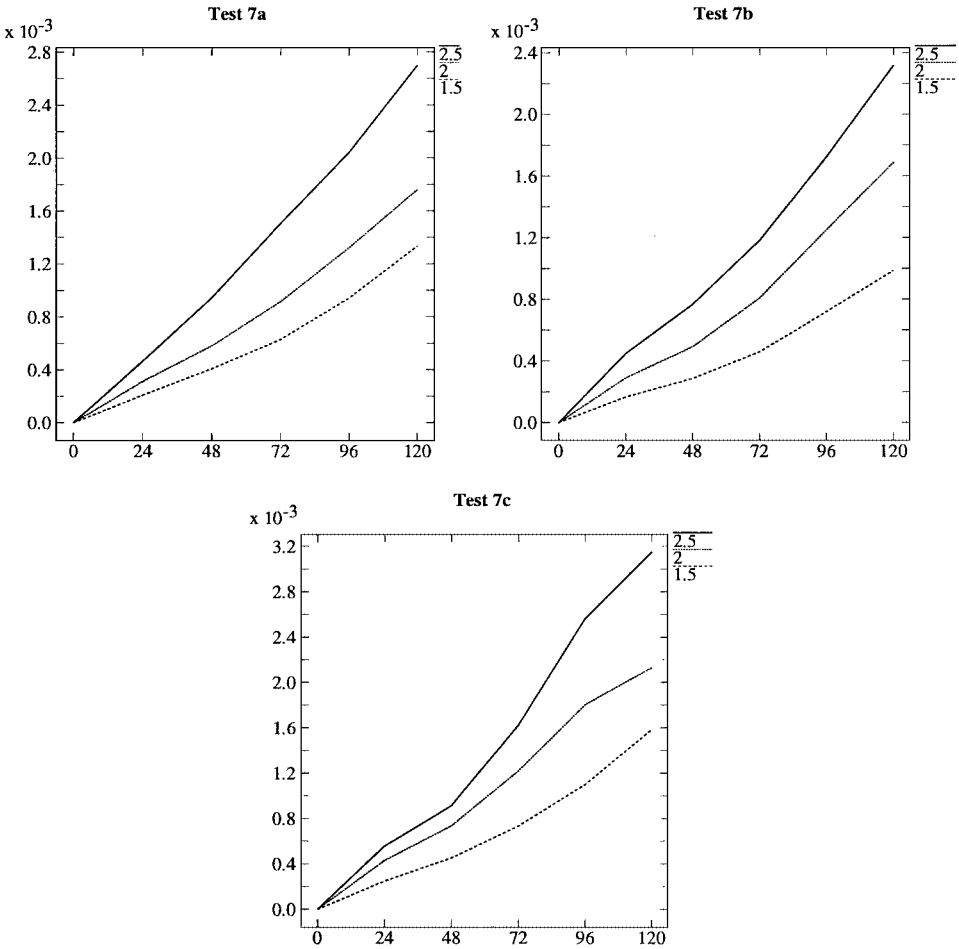

FIG. 7. Normalized l_2 height errors for tests 7a–7c with different resolutions (in degrees) as functions of forecast time (in hours).

Test case 7 is three real-data cases. The global normalized l_2 height errors for these tests with respect to the high-resolution (T213) spectral Eulerian model solution [8] are given in Figs. 7a–7c. One can see that the errors for the 2 degrees of resolution are better than those of solutions obtained with a spectral Eulerian model with a little bit higher equivalent resolution (T63, 1.875 degrees) and a time step four times smaller [8, Fig. 5.11]. For the resolution of 1.5 degrees, the error is smaller than for the equivalent T85 spectral model and is the same as for the model with a higher resolution, T106. The similar result was obtained for the Eulerian model based on fourth-order compact finite differences [20]. As was discussed in [20], it can be attributed to the fact that the spectral model can use at maximum two-thirds of its waves due to triangular truncation (in a Eulerian 3D model typically only half of all waves are retained). One can note again that the proposed scheme is two times more accurate on this test than the explicit Arakawa–Lamb model for the resolution of 2.5 degrees [22]. The uncertainty of the l_2 norm for this test is 0.00015 [22].

For one of these cases, namely for the initial data of 0000 UTC 21 December 1978, we also present the reference solution of the T213 model at day 5 of integration and the solution

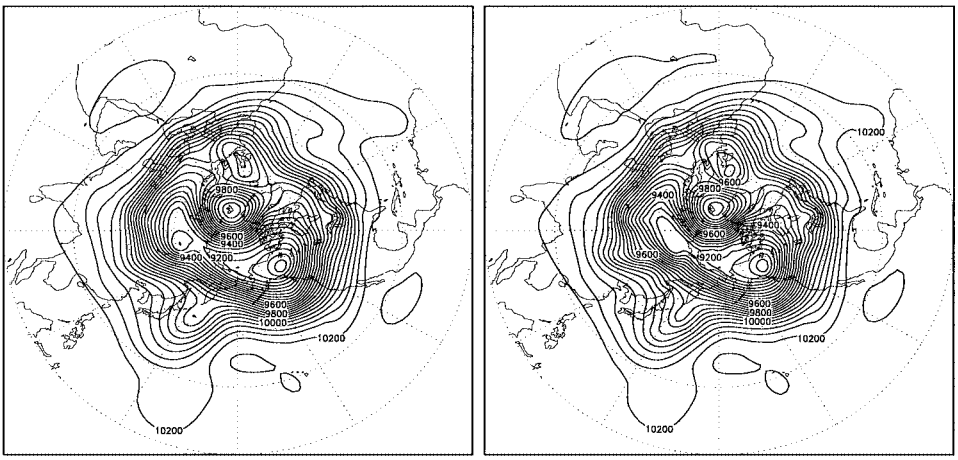

FIG. 8. Reference high-resolution solution at day 5 (left), and the solution of the model (2 degrees of resolution) on day 5 (right) for the 21 December 1978 case (test 7a). Decentering parameter, $\epsilon = 0.01$; diffusion coefficient, $K_D = 1 \times 10^{13}$ m^4/s.

given by our model with 2 degrees of resolution (Fig. 8). One can see that the solution near the northern pole is free of noise and agrees well with the reference solution.

This test was also repeated with the commonly used cubic Lagrangian interpolation to estimate quantities at the departure points of trajectories. In agreement with the results of the previous version of the model [26], the cubic Lagrangian interpolation gives larger errors than the spline interpolation (not shown). Further analysis has shown that the most significant response to the changes in interpolation is observed in the vorticity equation while other equations are sensitive, to a minor extent, to the type of interpolation.

5. CONCLUSIONS

The semi-Lagrangian representation of advection allows circumventing of the CFL restriction on time steps, which is especially severe for finite-difference models on the regular spherical latitude–longitude grid, making it possible to achieve high efficiency in these models.

The global semi-Lagrangian finite-difference shallow-water model was presented. The distinct features of this model are the use of vorticity and divergence as prognostic variables in conjunction with the fourth-order compact finite differences for discretization of the nonadvective terms on the unstaggered regular latitude–longitude grid. The key point of this approach is the solution of the Poisson equations on the sphere, which is necessary for reconstructing the velocity field from vorticity and divergence. The accurate and efficient direct solver for this problem was described. This solver uses fast Fourier transforms in the longitudinal direction. The solution of the elliptic problem arising in the semi-implicit time stepping algorithm and the horizontal diffusion of divergence are also carried out in Fourier space.

The proposed model is more expensive than the classical u–v second-order finite-difference semi-Lagrangian model using the staggered C grid, since we have to make additional interpolations of quantities at the departure points of trajectories and to reconstruct the velocity field from divergence and vorticity. However, in the full 3D version of the model,

including the parameterizations of the subgrid scale processes, the associated overhead is only 7.5% of the CPU time per time step. This increase in cost is offset by the increased accuracy of the model with respect to the classical u–v second-order finite-difference formulation on the staggered grid. On the other hand, the proposed model is more efficient than the spectral semi-Lagrangian model, especially for high resolutions, where the cost of the Legendre transforms in the spectral method grows dramatically.

The standard test set for shallow-water equations on the sphere was carried out with the presented model. The results show that it cannot compete with the spectral model on the simplest tests from this set where the solution can be obtained analytically by the spectral model. However, on more realistic tests it demonstrates the accuracy equal or superior to the Eulerian spectral model of equivalent resolution, with the time steps several times larger than for the latter.

The 3D version of the model already exists and recently successfully passed the 3-year integration with the prescribed analytic forcing [7]. These results will be published in a separate paper. The variable resolution in latitude is being implemented currently.

ACKNOWLEDGMENTS

This work was supported by EC INTAS Grant 96-2074, Russian RFBR Grant 01-05-64582, and a grant from the fifth competition of the Commission for support of young scientists, Russian Academy of Sciences, 1997. The comments of anonymous referees helped to improve the paper. The isolines were produced with the help of a GrADS package.

REFERENCES

1. J. R. Bates, F. H. M. Semazzi, R. W. Higgins, and S. R. M. Barros, Integration of the shallow water equations on the sphere using a vector semi-Lagrangian scheme with a multigrid solver, *Mon. Weather Rev.* **118**, 1615 (1990).
2. J. R. Bates, Yong Li, A. Brandt, S. F. McCormick, and J. Ruge, A global shallow-water numerical model based on the semi-Lagrangian advection of potential vorticity, *Q. J. R. Meteorol. Soc.* **121**, 1981 (1995).
3. H.-B. Cheong, Application of double Fourier series to the shallow water equations on a sphere, *J. Comput. Phys.* **165**, 261 (2000), doi:10.1006/jcph.2000.6615.
4. I. G. Gospodinov, V. G. Spirodonov, P. Benard, and J.-F. Geleyn, A refined semi-Lagrangian vertical trajectory scheme applied to a hydrostatic atmospheric model, *Q. J. R. Meteorol. Soc.* **128**, 323 (2002).
5. F. X. Giraldo, Lagrange-Galerkin methods on spherical geodesic grids: The shallow water equations, *J. Comput. Phys.* **160**, 336 (2000), doi:10.1006/jcph.2000.6469.
6. M. Hortal, Aspects of the numerics of the ECMWF model, in *Recent Developments in Numerical Methods for Atmospheric Modelling, Proceedings of the ECMWF Seminar, 7–11 September, 1998* (ECMWF, Reading, UK, 1999), p. 127.
7. I. M. Held and M. J. Suarez, A proposal for the intercomparison of the dry dynamical cores of atmospheric general circulation models, *Bull. Am. Met. Soc.* **75**, 1825 (1994).
8. R. Jakob-Chien, J. J. Hack, and D. L. Williamson, Spectral transform solutions to the shallow water test set, *J. Comput. Phys.* **119**, 164 (1995), doi:10.1006/jcph.1995.1125.
9. S. K. Lele, Compact finite difference schemes with spectral-like resolution, *J. Comput. Phys.* **103**, 16 (1992).
10. Y. Li, S. Moorthi, and J. R. Bates, *Direct Solution of the Implicit Formulation of Fourth Order Horizontal Diffusion for Gridpoint Models on the Sphere*, NASA GLA Technical Report Series in Atmospheric Modelling and Data Assimilation, Vol. 2 (1994).
11. Y. Li and J. R. Bates, A study of the behavior of semi-Lagrangian models in the presence of orography, *Q. J. R. Meteorol. Soc.* **122**, 1675 (1996).

12. P. Lynch and X.-Y. Huang, Initialization of the HIRLAM model using a digital filter, *Mon. Weather Rev.* **120**, 1019 (1992).
13. A. McDonald, The origin of noise in semi-Lagrangian integrations, in *Recent Developments in Numerical Methods for Atmospheric Modelling, Proceedings of the ECMWF Seminar, 7–11 September, 1998* (ECMWF, Reading, UK, 1999), p. 308.
14. S. Moorthi and R. W. Higgins, Application of fast Fourier transforms to the direct solution of a class of two-dimensional separable elliptic equations on the sphere, *Mon. Weather Rev.* **121**, 290 (1993).
15. B. Neta and R. T. Williams, Rossby wave frequencies and group velocities for finite element and finite difference approximations to the vorticity-divergence and primitive forms of the shallow water equations, *Mon. Weather Rev.* **117**, 1439 (1989).
16. B. V. Numerov, *Astron. Nachr.* **230**, 359 (1927).
17. D. A. Randall, Geostrophic adjustment and the finite-difference shallow water equations, *Mon. Weather Rev.* **122**, 1371 (1994).
18. M. Rochas, *ARPEGE Documentation*, Part 2, Chap. 6, available from Météo-France, Toulouse, France (1990).
19. H. Ritchie and M. Tanguay, A comparison of spatially averaged Eulerian and semi-Lagrangian treatments of mountains, *Mon. Weather Rev.* **124**, 167 (1996).
20. W. F. Spotz, M. A. Taylor, and P. N. Swarztrauber, Fast shallow-water equations solvers in latitude-longitude coordinates, *J. Comput. Phys.* **145**, 432 (1998), doi:10.1006/jcph.1998.6026.
21. A. Staniforth and J. Côté, Semi-Lagrangian integration schemes for atmospheric models—A review, *Mon. Weather Rev.* **119**, 2206 (1991).
22. M. Taylor, J. Tribbia, and M. Iskandarani, The spectral element method for the shallow water equations on the sphere, *J. Comput. Phys.* **130**, 92 (1997), doi:10.1006/jcph.1996.5554.
23. C. Temperton and A. Staniforth, An efficient two-time-level semi-Lagrangian semi-implicit integration scheme, *Q. J. R. Meteorol. Soc.* **113**, 1025 (1987).
24. C. Temperton, An overview of recent developments om numerical methods for atmospheric modelling, in *Recent Developments in Numerical Methods for Atmospheric Modelling, Proceedings of the ECMWF Seminar, 7–11 September, 1998* (ECMWF, Reading, UK, 1999), p. 1.
25. J. Thuburn and Y. Li, Numerical simulations of Rossby-Haurwitz waves, *Tellus* **52A**, 181 (2000).
26. M. Tolstykh, Global semi-Lagrangian atmospheric model based on compact finite-differences, in *Proceedings of the 3rd ECCOMAS Computational Fluid Dynamics Conference, Paris, France, September, 1996* (Wiley, Chichester/New York, 1996), p. 14.
27. M. Tolstykh, Implementation of the fourth-order horizontal diffusion in Fourier space in the variable resolution spectral model, in *Research Activities in Atmospheric and Oceanic Modelling*, edited by A. Staniforth, WMO WGNE Rep. N 25, WMO/TD-792, 3.40–3.41 (World Meteorological Organisation, Geneva, Switzerland, 1997).
28. M. Tolstykh, Atmospheric circulation and weather prediction models using semi-Lagrangian approach and high-order compact finite-differences, *Russ. J. Numer. Anal. Math. Model.* **13**(6), 551 (1998).
29. M. Tolstykh, Semi-Lagrangian high resolution atmospheric model for numerical weather prediction, *Russ. Meteorol. Hydrol.* **4**, 1 (2001).
30. V. V. Voevodin and E. E. Tyrtyshnikov, *Computational Processes with Toeplitz Matrices* (Nauka, Moscow, 1987), p. 86 (Russian).
31. D. L. Williamson and P. J. Rasch, Two-dimensional semi-Lagrangian transport with shape-preserving interpolation, *Mon. Weather Rev.* **117**, 102 (1989).
32. D. L. Williamson, J. B. Drake, J. J. Hack, R. Jakob, and P. N. Swarztrauber, A standard test set for numerical approximations to the shallow water equations in spherical geometry, *J. Comput. Phys.* **102**, 211 (1992).
33. D. L. Williamson and J. G. Olson, A comparison of semi-Lagrangian and Eulerian polar climate simulation, *Mon. Weather Rev.* **126**, 991 (1998).
34. K. Yessad, Semi-Lagrangian computations in the cycle Cy16 of ARPEGE/IFS, Météo-France Internal Report (1997).